

A deterministic projector configuration interaction approach for the ground state of quantum many-body systems

Tianyuan Zhang¹ and Francesco A. Evangelista^{1, a)}

Department of Chemistry and Cherry L. Emerson Center for Scientific Computation, Emory University, Atlanta, Georgia 30322, USA

In this work we propose a novel approach to solve the Schrödinger equation which combines projection onto the ground state with a path-filtering truncation scheme. The resulting projector configuration interaction (PCI) approach realizes a deterministic version of the full configuration interaction quantum Monte Carlo (FCIQMC) method [Booth, G. H.; Thom, A. J. W.; Alavi, A. *J. Chem. Phys.* **2009**, *131*, 054106]. To improve upon the linearized imaginary-time propagator, we develop an optimal projector scheme based on an exponential Chebyshev expansion in the limit of an infinite imaginary time step. After writing the exact projector as a path integral in determinant space, we introduce a path filtering procedure that truncates the size of the determinantal basis and approximates the Hamiltonian. The path filtering procedure is controlled by one real threshold that determines the accuracy of the PCI energy and is not biased towards any determinant. Therefore, the PCI approach can equally well describe static and dynamic electron correlation. This point is illustrated in benchmark computation on N₂ at both equilibrium and stretched geometries. In both cases, the PCI achieves chemical accuracy with wave functions that contain less than 0.5% of the full CI space. We also report computations on the ground state of C₂ with up to quadruple- ζ basis sets and wave functions as large as 200 million determinants, which allow a direct comparison of the PCI, FCIQMC, and density matrix renormalization group (DMRG) methods. The size of the PCI wave function grows modestly with the number of unoccupied orbitals and its accuracy may be tuned to match that of FCIQMC and DMRG.

I. INTRODUCTION

The full configuration interaction (FCI) approach provides the exact solution to the electronic Schrödinger equation within a finite one-particle basis set.¹ However, since the number of FCI wave function parameters grows rapidly with system size, this approach is only feasible for few electrons distributed in a small number of orbitals.² Contrary to what is suggested by this observation, a large body of evidence has been amassed that shows that the information content of *molecular* wave functions is just a small fraction of the size of the FCI basis.³ For example, for wave functions dominated by one Slater determinant, truncated coupled cluster theory can recover a large fraction of the dynamical correlation energy at a cost that is polynomial in the number of electrons.⁴ However, in the case of strongly correlated electrons, the problem of finding general polynomial-scaling wave function methods is still open.^{5,6}

Several strategies have been suggested to overcome the exponential cost of FCI and FCI performed in a complete active space (CASCI), including selected CI approaches that truncate FCI space,^{7–21} tensor factorization,^{22–39} alternative configuration interaction and coupled cluster methods,^{40–43} symmetry breaking and restoration,^{44–46} and Monte-Carlo methods.^{47–63} Recently, Monte-Carlo methods that stochastically sample the wave function in the space of Slater determinants have received wide attention. The Monte-Carlo CI method (MCCI) uses stochastic sampling to find an optimal space of orthogonal Slater determinants.^{47–51} MCCI may be viewed as a stochastic version of selected CI since at each

iteration the energy is obtained by diagonalizing the Hamiltonian is a subset of the FCI space.^{7–10} Another stochastic method is the auxiliary-field QMC (AFQMC) approach.^{52–54,56} AFQMC uses a projector formalism and differs from MCCI in its use of non-orthogonal Slater determinants and the fact that the wave function is sampled stochastically. Deterministic analogs of the AFQMC approach have also been developed, including the path-integral renormalization group method^{64,65} and the non-orthogonal multicomponent adaptive greedy iterative compression approach of McClean and Aspuru-Guzik.⁶⁶

An alternative to the MCCI and AFQMC methods is the FCI Quantum Monte-Carlo (FCIQMC) method developed by Alavi and co-workers.^{57–63} FCIQMC is a projector Monte-Carlo method that samples the imaginary-time propagator in a space of orthogonal Slater determinants. By working in a basis of Slater determinants, FCIQMC can more easily account for the annihilation of walkers of different sign. This feature ameliorates the sign problem, but a large number of walkers are necessary to accurately sample the FCI space of determinants. The initiator approximation⁵⁸ reduces the number of walkers required in FCIQMC and increases the sign coherence of the sampling. Furthermore, a semi-stochastic version of FCIQMC (SFCIQMC) was later introduced,^{67–69} which shows that treating part of the imaginary-time projection deterministically accelerates convergence and reduces statistical uncertainty.

The improvements to the performance of FCIQMC brought by treating part of determinant space deterministically raises the interesting question of whether a fully deterministic projector method might be even more advantageous. As pointed out by Tubman and co-workers,⁷⁰ the stochastic dynamics of FCIQMC reinterpreted in a deterministic way corresponds to a truncation

^{a)}Electronic mail: francesco.evangelista@emory.edu

criterion for selected CI. In this work, we demonstrate an alternative route to create a deterministic analog of FCIQMC. An important feature of our new method is the use of a projection scheme that simultaneously selects an optimal CI space and approximately diagonalizes the Hamiltonian. The resulting computational method is named projector configuration interaction (PCI). The PCI approach automatically identifies the most important determinants that contribute to the ground state wave function, therefore, it can treat both dynamic and static electron correlation.

The PCI methods presents two major differences with respect to FCIQMC. As in other projector Monte-Carlo methods, FCIQMC relies on a linearized approximation to the imaginary-time projector obtained by Taylor expansion. One of the major drawbacks of this approximation is that a small time step is required to guarantee convergence to the ground state, the length of which is bound by the inverse spectral radius of the Hamiltonian. Following the work of Kosloff and Tal-Ezer⁷¹, we overcome this limitation by using a Chebyshev expansion of the exponential projector.^{72–76} In particular, we consider the *wall*-Chebyshev projector, which is derived from the Chebyshev representation of the imaginary-time propagator in the limit of an infinite time step. In this respect, our goal is analogous to that of the t expansion method, in which the $t \rightarrow \infty$ limit of the imaginary-time propagator is expressed using Padé approximants.⁷⁷ The *wall*-Chebyshev generator is shown to be equivalent to a power method with alternating shifts, and it is more efficient than the corresponding Taylor and Chebyshev expansions of the exponential projector. We also address the issue of replacing Monte-Carlo sampling with a deterministic truncation of the determinant space. Since projection onto the ground state may be viewed as a path-integral scheme, we apply the idea of path filtering^{78–81} in order to truncate CI space and control accuracy. In the PCI, path filtering is applied to screen excited determinants generated by projection onto the ground state. Path filtering is controlled by one threshold parameter, and as a consequence, the PCI forms a family of one-parameter theories that are systematically improvable and equivalent to FCI when path filtering is suppressed.

The paper is organized in the following way. In section 2, we introduce the formalism of ground state projection, Chebyshev fitting of the imaginary-time propagator, and path filtering. Section 3 details the PCI algorithm and our implementation and analyzes the sources of error in the PCI approach. In section 4 we demonstrate the ability of PCI to adapt to various regimes of electron correlation by applying it to the dissociation of N_2 . In the same section, we study the scaling of the PCI cost with respect to basis set size and the size consistency error introduced by the path-filtering approximation.

II. THEORY

A. General formalism of ground state projection

Given the Hamiltonian operator \hat{H} , we write its eigenvalues and eigenfunctions as E_i and Ψ_i , respectively. Within a finite computational basis, the Hamiltonian is assumed to have N eigenfunctions, and its spectral radius (R) is defined as the difference between the largest (E_{N-1}) and smallest (E_0) eigenvalues divided by two:

$$R = \frac{E_{N-1} - E_0}{2} \quad (1)$$

The goal of projector CI (PCI) is to obtain the ground state wave function Ψ_0 starting from a trial wave function Ω via a projector operator \hat{P}_0 :

$$|\Psi_0\rangle = N_P \hat{P}_0 |\Omega\rangle \quad (2)$$

The only assumption concerning the trial wave function is that its overlap with the exact ground state is not zero, that is $\langle \Omega | \Psi_0 \rangle \neq 0$. In Eq. (2), N_P is a normalization factor introduced to guarantee that $\langle \Psi_0 | \Psi_0 \rangle = 1$ and the projector operator \hat{P}_0 is assumed to be idempotent ($\hat{P}_0^2 = \hat{P}_0$).

We restrict our discussion to a class of projectors that can be written as the infinite product:

$$\hat{P}_0 = \lim_{n \rightarrow \infty} g^n(\hat{H}) \quad (3)$$

where $g(\cdot)$ is the *generator of the projector* \hat{P}_0 (also abbreviated as *generator* in the following). The projector generator is assumed to be a real function $g : \mathbb{R} \rightarrow \mathbb{R}$ extended to the domain of Hermitian operators. Given a generic state vector $|\Omega\rangle$, it may be decomposed as a sum over the eigenfunctions of the Hamiltonian as:

$$|\Omega\rangle = \sum_i c_i |\Psi_i\rangle \quad (4)$$

so that the action of the projector generator $g(\hat{H})$ onto $|\Omega\rangle$ may be written out:

$$g(\hat{H}) |\Omega\rangle = \sum_i c_i g(\hat{H}) |\Psi_i\rangle = \sum_i g(E_i) c_i |\Psi_i\rangle \quad (5)$$

Thus, the application of a generator onto a trial state vector leads to a new state vector in which the coefficient that multiplies each $|\Psi_i\rangle$ is amplified by a factor $g(E_i)$, where E_i is the eigenvalue corresponding to $|\Psi_i\rangle$.

For an appropriately chosen generator, the repeated application of $g(\hat{H})$ may be used to amplify the coefficient of the ground state wave function and reduce that of excited states. A necessary condition for the generator to project a state onto Ψ_0 is to satisfy the inequality:

$$|g(E_0)| > |g(x)| \quad \forall x \in (E_0, E_{N-1}] \quad (6)$$

so that the relative weight of the excited states is reduced by a factor $q_i = g(E_i)/g(E_0)$:

$$g(\hat{H})|\Omega\rangle = c_0|\Psi_0\rangle + \sum_{i=1}^{N-1} q_i c_i |\Psi_i\rangle \quad |q_i| < 1 \quad (7)$$

where without loss of generality, we have assumed that $g(x)$ is scaled so that $g(E_0) = 1$. In practical applications, the range of \hat{H} is unknown, but as discussed in section III, one may obtain upper bounds of E_0 and E_{N-1} (here denoted \tilde{E}_0 and \tilde{E}_{N-1}). In this case, it is convenient to work with generators that decrease monotonically in the left-neighborhood of \tilde{E}_0 , that is for any two points $x, y \in [E_0, \tilde{E}_0]$:

$$|g(x)| > |g(y)| \text{ if } x < y \quad (8)$$

When the monotonicity condition expressed by Eq. (8) is satisfied, the projector is guaranteed to converge to the ground state even if E_0 and E_{N-1} are approximated with their respective upper bound estimates. Therefore, in the following discussion we do not distinguish \tilde{E}_0 from E_0 .

B. Rate of convergence of generators.

The repeated application of the generator onto a trial wave function $\Omega^{(0)}$ generates a sequence of vectors:

$$|\Omega^{(n)}\rangle = g^n(\hat{H})|\Omega^{(0)}\rangle \quad (9)$$

which in the limit of n that goes to infinity converges to the exact ground state:

$$|\Psi_0\rangle = \lim_{n \rightarrow \infty} |\Omega^{(n)}\rangle \quad (10)$$

The asymptotic rate of convergence of this sequence is defined as:

$$\mu = \lim_{n \rightarrow \infty} \frac{\|\Omega^{(n+1)} - \Psi_0\|}{\|\Omega^{(n)} - \Psi_0\|} = \max_i |q_i| \quad (11)$$

and is given by the q_i factor with the largest absolute value.

When the rate of convergence is controlled by the first excited state, that is $\mu = |q_1|$, and the energy difference $E_1 - E_0$ is small compared to the spectral radius, then we can approximate μ as:

$$\mu = \left| \frac{g(E_1)}{g(E_0)} \right| \approx |1 + g'(E_0) \cdot (E_1 - E_0)| \quad (12)$$

where $g'(E_0)$ is the first derivative of $g(x)$ at E_0 . Hence, we can define the convergence factor γ for $g(x)$ as

$$\gamma = -g'(E_0) \quad (13)$$

It is possible to show that the number of times one must apply $g(\hat{H})$ to a trial wave function in order to achieve

a certain level of accuracy is inversely proportional to γ . Therefore, the convergence factor provides a quantitative estimate of the numerical efficiency of a generator. Generators with large convergence factors are in general preferable as they are expected to reduce the computational cost of the PCI. The parameters that enter the definition of all the generators discussed in this work and their corresponding convergence factor are summarized in Table I.

C. Taylor and Chebyshev expansions of the imaginary-time propagator

The projector generator corresponding to the imaginary-time propagator, $\lim_{\beta \rightarrow \infty} e^{-\beta(\hat{H}-E_0)}$, is the exponential generator (g_{exp}), defined as:

$$g_{\text{exp}}(x) = e^{-\tau(x-E_0)} \quad (14)$$

This generator satisfies both conditions Eqs. (6) and (8). Nevertheless, it is not expressed as a polynomial of the Hamiltonian and therefore, to make its evaluation computationally viable it must be approximated with a polynomial expansion. To evaluate the projector based on the exponential generator [Eq. (14)] it is necessary to expand $g_{\text{exp}}(x)$ into a polynomial series.

An m -th order Taylor expansion of $g_{\text{exp}}(x)$ centered around E_0 yields the generator:

$$g_{\text{expTaylor}}(x) = \sum_{k=0}^m \frac{1}{k!} (-\tau)^k (x - E_0)^k \quad (15)$$

which has convergence factor $\gamma_{\text{expTaylor}} = \tau$ independent of the truncation order m . Consequently, there is not gain in efficiency when $g_{\text{expTaylor}}(x)$ is expanded beyond $m = 1$. More importantly, the Taylor expansion is only accurate near E_0 , and since the error grows as a power of $\tau(x - E_0)$, a very small value of τ may be required to satisfy the necessary condition for the convergence of the projector [see Eq. (6)].

Note, that the first-order Taylor expansion of the exponential:

$$g_{\text{linear}}(x) = 1 - \tau(x - E_0) = -\tau(x - s) \quad (16)$$

is equivalent to a power method with shift $s = E_0 + \frac{1}{\tau}$. In order to converge to the ground state wave function, the shift must be chosen to satisfy $s > R$. The corresponding convergence factor is bound by the inverse of the spectral range of the Hamiltonian:

$$\gamma_{\text{linear}} = \tau < \frac{1}{R} \quad (17)$$

An alternative approximation of the exponential with better error control is an expansion in terms of Chebyshev polynomials (for example, see Refs. 71 and 76). Following Kosloff and Tal-Ezer,⁷¹ we write the m -th order

Table I. Comparison of different projector generators. The form of the projector generator $[g(x)]$ and convergence factor (γ) is given as a function of the time step (τ), the spectral radius of the Hamiltonian (R), and the order of the polynomial expansion (m).

Generator	Parameters	$g(x)$	Convergence factor (γ)
Exponential	τ	$e^{-\tau(x-E_0)}$	τ
Linear	τ	$1 - \tau(x - E_0)$	$\tau < \frac{1}{R}^*$
Exp-Taylor	τ, m	$\sum_{k=0}^m \frac{1}{k!} (-\tau)^k (x - E_0)^k$	$\tau < \frac{m+1}{2R}^{**}$
Exp-Chebyshev	τ, R, m	$C_m(\tau R) \sum_{k=0}^m (2 - \delta_{k0}) I_k(\tau R) T_k \left(-\frac{x - E_0 - R}{R} \right)$	$\frac{\sum_{k=1}^m 2I_k(\tau R) k^2}{R \sum_{k=0}^m (2 - \delta_{k0}) I_k(\tau R)} < \frac{m(m+1)}{3R}$
Wall-Chebyshev	R, m	$\frac{1}{2m+1} \sum_{k=0}^m (2 - \delta_{k0}) T_k \left(-\frac{x - E_0 - R}{R} \right)$	$\frac{m(m+1)}{3R}$

* In order to converge onto the ground state wave function, the time step must satisfy the condition: $\tau < \frac{1}{R}$.

** In order to converge onto the ground state wave function, the time step must satisfy the condition: $|\sum_{k=0}^m \frac{1}{k!} (-\tau)^k (2R)^k| < 1$. From this expression one may derive the upper bound: $\tau < \frac{m+1}{2R}$.

Chebyshev polynomial fitting of the exponential generator as:

$$g_{\text{expCh}}(x) = C_m(\tau R) \sum_{k=0}^m (2 - \delta_{k0}) I_k(\tau R) T_k \left(-\frac{x - E_0 - R}{R} \right) \quad (18)$$

where $C_m(\tau R) = 1 / (\sum_{k=0}^m (2 - \delta_{k0}) I_k(\tau R))$ is a scaling factor that guarantees $g_{\text{expCh}}(E_0) = 1$, δ_{k0} is a Kronecker delta, I_k is the k -th modified Bessel function of the first kind, and T_k is the k -th order Chebyshev polynomial.

Figure 1A shows first- and second-order Taylor and Chebyshev expansions of the exponential evaluated for $\tau = 2 E_h^{-1}$ in the range $[-1, 1] E_h$. This plot illustrates the points made above: i) the Taylor expansion of the exponential is accurate only near the expansion point (in this case $E_0 = -1 E_h$) and ii) the Chebyshev expansion is well behaved on the entire range. Figure 1B shows the Chebyshev expansion for the same range but with $\tau = 10 E_h^{-1}$. In this case the fitting error is larger and the convergence of the Chebyshev expansion with respect to the order m is slower than the case $\tau = 2 E_h^{-1}$. Nevertheless, even though the Chebyshev expansion for $\tau = 10 E_h^{-1}$ does not accurately match the exponential function, it is still a valid projector generator since it satisfies Eqs. (6) and (8).

D. An improved generator: the wall generator and its Chebyshev expansion.

In the previous subsection we discussed how to improve the accuracy of the Taylor expansion of the exponential generator via Chebyshev fitting. Ideally, the best projec-

tor generator is the the *wall* function, defined as:

$$g_{\text{wall}}(x) = \begin{cases} 0 & \text{for } x > E_0 \\ 1 & \text{for } x = E_0 \\ \infty & \text{for } x < E_0 \end{cases} \quad (19)$$

This generator may be viewed as the $\tau \rightarrow \infty$ limit of the exponential generator:

$$g_{\text{wall}}(x) = \lim_{\tau \rightarrow \infty} e^{-\tau(x-E_0)} \quad (20)$$

Despite the fact that neither definitions of $g_{\text{wall}}(x)$ are computationally viable, we can still approximate the wall generator using a Chebyshev expansion, by taking the $\tau \rightarrow \infty$ limit of the m -th order exponential Chebyshev generator:

$$\begin{aligned} g_{\text{wallCh}}(x) &= \lim_{\tau \rightarrow \infty} g_{\text{expCh}}(x) \\ &= \frac{1}{2m+1} \sum_{k=0}^m (2 - \delta_{k0}) T_k \left(-\frac{x - E_0 - R}{R} \right) \end{aligned} \quad (21)$$

where we used the fact that $\lim_{\tau \rightarrow \infty} I_{k+1}(\tau R) / I_k(\tau R) = 1$.⁸² Note that this polynomial is a special case of the Chebyshev expansion of the delta distribution with the origin translated to the lower bound of the fitting range.⁷²⁻⁷⁵

The wall-Chebyshev generators of order 1, 2, 4, and 8 are plotted in Figure 1C. An important property of the wall-Chebyshev generator is that for values of x less than E_0 these functions are monotonic and diverge when $x \rightarrow -\infty$. Therefore they satisfy Eq. (8) and are able to converge onto the ground state even when the range of \hat{H} is not known precisely.

The Chebyshev expansion of the wall generator may

shown to converge with factor

$$\gamma_{\text{wallCh}} = \frac{m(m+1)}{3R} \quad (22)$$

which is the largest one among all the polynomial generators discussed in this work. It is important to note that although we can design generators with even larger convergence factors, an efficient generator must also efficiently suppress high energy excited states. For example, the Chebyshev generator, defined as $g_{\text{Ch}}(x) =$

$T_k\left(-\frac{x-E_0-R}{R}\right)$ gives $\gamma_{\text{Ch}} = \frac{m^2}{R}$, which is larger than the convergence factor of the generators discussed previously. However, the convergence of the projector generated by $g_{\text{Ch}}(x)$ is slow because the coefficients of high energy excited states are not efficiently reduced.

In each projection generation step, an m -th order wall-Chebyshev generator involves the application of the Hamiltonian m times, therefore, it has a cost that is m times that of the linear generator (power method). Consequently, the theoretical relative acceleration with respect to the most efficient linear generator ($\tau_{\text{linear}} = 1/R$) is:

$$\frac{\gamma_{\text{wallCh}}}{m\gamma_{\text{linear}}} = \frac{m+1}{3} \quad (23)$$

For instance, an 8th-order wall-Chebyshev generator has a computational cost that is a third of the linear generator with the largest allowed value of τ ($1/R$).

An important property of the m -th order $g_{\text{wallCh}}(x)$ generator is that it has m distinct real roots in the range (E_0, E_{N-1}) . Therefore, it can be decomposed as a product of m linear generators with real shifts:

$$g_{\text{wallCh}}(x) = \prod_{i=1}^m \frac{x - s_i}{E_0 - s_i} \quad (24)$$

where the shifts s_i are the zeros of $g_{\text{wallCh}}(x)$. It is easy to show that the zeros of $g_{\text{wallCh}}(x)$ can be expressed in closed form as:

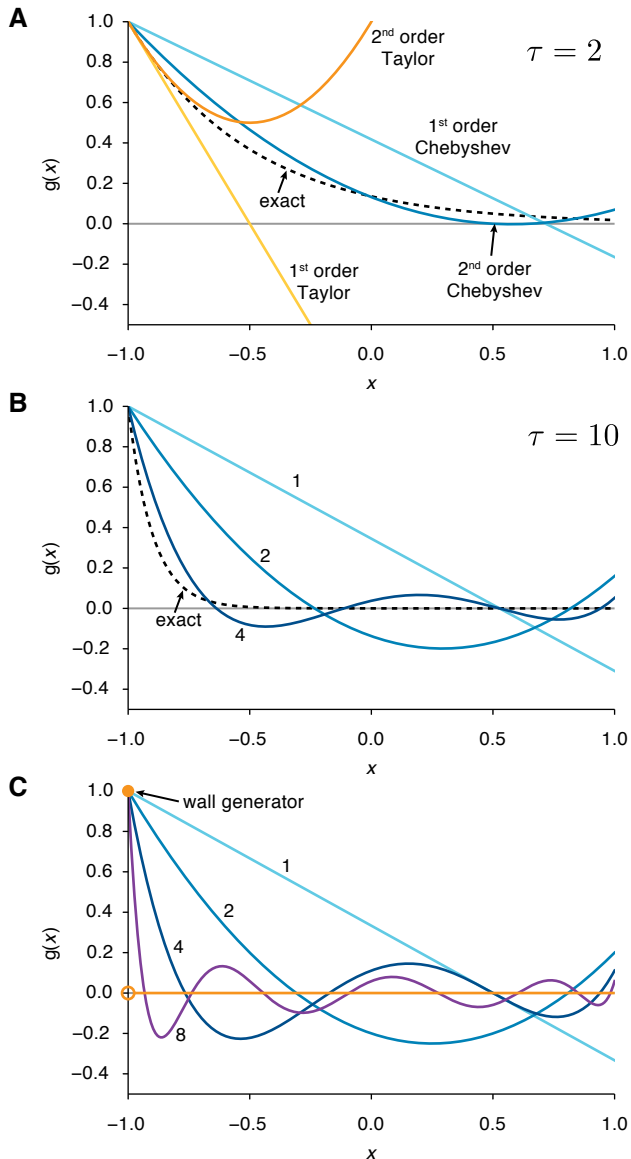
$$s_i = E_0 + R \left(1 - \cos \frac{i}{m + \frac{1}{2}} \pi\right) \quad (25)$$

Eq. (24) allows us to implement the wall generator as a product of linear generators applied successively onto a state vector. Hence, the projector associated with the wall generator may be interpreted as an optimized power method that uses a sequence of energy shifts. Besides its high efficiency, there are two other advantages of the wall-Chebyshev generator: i) Only two vectors (previous and current) need to be stored during the calculation, in contrast to three vectors necessary for the exp-Chebyshev generator (previous, current and accumulator) and ii) the wall-Chebyshev generator is numerically more stable than the exp-Chebyshev generator since for $\tau \rightarrow \infty$ the numerical evaluation of Bessel functions introduces numerical errors.

E. Determinant selection via path filtering.

The projector CI discussed in Section II A provides an alternative approach to finding the exact ground state. In this section we show how to combine this methods with path filtering to generate an approach that diagonalizes the Hamiltonian in an optimal subset of FCI space. We discuss path filtering only for the case of the linear generator and report details for higher-order polynomial generators in appendix A.

Figure 1. Polynomial approximations of the exponential generator [Eq. (14)] and the $\tau \rightarrow \infty$ limit of the exponential generator (wall generator) [Eq. (20)] plotted in the range $[-1, 1] E_h$. (A) Taylor and Chebyshev approximation of the exponential generator for $\tau = 2 E_h^{-1}$ at order 1 and 2. (B) Chebyshev approximation of the exponential generator for $\tau = 10 E_h^{-1}$ at order 1, 2, and 4. (C) Chebyshev approximation of the wall generator at order 1, 2, 4, and 8.



Consider a normalized trial state $\Omega^{(n)}$ that approximates the exact ground state in the subset $S^{(n)}$ of FCI space:

$$|\Omega^{(n)}\rangle = \sum_{\Phi_J \in S^{(n)}} C_J^{(n)} |\Phi_J\rangle \quad (26)$$

where $C_J^{(n)}$ is the coefficient of determinant $|\Phi_J\rangle$ at the n -th step. The action of the linear generator onto $\Omega^{(n)}$ leads to a new state $\tilde{\Omega}^{(n+1)}$:

$$g_{\text{linear}}(\hat{H}) |\Omega^{(n)}\rangle = |\tilde{\Omega}^{(n+1)}\rangle = \sum_I \tilde{C}_I^{(n+1)} |\Phi_I\rangle \quad (27)$$

where, in general, the vector of coefficients $\tilde{C}_I^{(n+1)}$ is not normalized. The coefficients of $\tilde{C}_I^{(n+1)}$ may be expressed as a sum over *spawning amplitudes*, $A_{IJ}^{(n+1)}$:

$$\begin{aligned} \tilde{C}_I^{(n+1)} &= \langle \Phi_I | 1 - \tau(\hat{H} - E_0) |\Omega^{(n)}\rangle \\ &= \tau \sum_{\Phi_J \in S^{(n)}} A_{IJ}^{(n+1)} \end{aligned} \quad (28)$$

where $A_{IJ}^{(n+1)}$ is defined as:

$$A_{IJ}^{(n+1)} = \frac{1}{\tau} \langle \Phi_I | 1 - \tau(\hat{H} - E_0) |\Phi_J\rangle C_J^{(n)} \quad (29)$$

The spawning amplitude has the units of a rate and represents the contribution of the Φ_J component of $\Omega^{(n)}$ that “flows” to the coefficient of Φ_I for state $\tilde{\Omega}^{(n+1)}$.

The repeated application of the generator onto a trial function generates paths in FCI space that may be filtered (approximated) by thresholding the spawning amplitude. To this end we introduce a *spawning threshold* η and truncate the off-diagonal spawning amplitude as:

$$A_{IJ}^{(n)}(\eta) = \begin{cases} A_{IJ}^{(n)} & \text{if } I = J \\ A_{IJ}^{(n)} \Theta(|A_{IJ}^{(n)}| - \eta) & \text{if } I \neq J \end{cases} \quad (30)$$

where $\Theta(x)$ is the Heaviside step function. Consequently, the PCI update equations for the wave function coefficients are:

$$\tilde{C}_I^{(n+1)} = \tau \sum_{\Phi_J \in S^{(n)}} A_{IJ}^{(n+1)}(\eta) \quad (31)$$

and the determinant set at step $n+1$ includes only those elements of the FCI space that may be reached from $S^{(n)}$ via non-zero amplitudes:

$$S^{(n+1)} = \{\Phi_I : \exists \Phi_J \in S^{(n)}, A_{IJ}^{(n+1)}(\eta) \neq 0\} \quad (32)$$

In other words, a determinant is included in $S^{(n+1)}$ when there is at least one spawning amplitude that is larger than the spawning threshold. Note that this selection criterion is analogous to the one used in heat-bath sampling⁸³ and accounts both for the weight of a parent

determinant, via the factor $C_J^{(n)}$, and for the coupling between parent and spawned determinant, via the matrix element of the linearized generator $\langle \Phi_I | 1 - \tau(\hat{H} - \epsilon) |\Phi_J\rangle$.

In order to further reduce the computation cost, the so-called initiator approximation⁵⁸ is introduced in FCIQMC, which imposes a screening of the determinants that may be spawned. Translated in the language of the PCI approach, the initiator approximation is equivalent to a path-filtering procedure in which the screening is done according to the absolute value of a determinant coefficient $[C_I^{(n)}]$. Thus, the initiator approximation considers only the importance of the parent determinant, while as already mentioned selection performed by the PCI considers both the importance of parent determinants and the coupling between parent and spawned determinants.

F. Sources of errors in the PCI method

When compared to FCI, the PCI method introduces two types of error. The first, the truncation error, is connected to the use of a subset of the full Hilbert space of determinants, and also affects selected CI methods. Note that the truncation error does not affect methods like FCIQMC, which in principle can sample the entire Hilbert space. The second type of error, the path filtering error, arises from approximating the action of the generator onto a state vector via Eqs. (30) and (31). The path filtering error may be viewed as arising from the diagonalization of an approximate Hamiltonian (\tilde{H}), which results from the path filtering procedure:

$$\tilde{H}_{IJ}^{(n)} = \begin{cases} H_{IJ} & \text{if } A_{IJ}^{(n)}(\eta) \neq 0 \\ 0 & \text{if } A_{IJ}^{(n)}(\eta) = 0 \end{cases} \quad (33)$$

Obviously, $\tilde{H}^{(n)}$ depends on the current wave function, and it is not guaranteed to be symmetric since in general $A_{IJ}^{(n)}(\eta) \neq A_{JI}^{(n)}(\eta)$. In the PCI, the path filtering error arises from the fact that the wave function coefficient vector is the right eigenvector of $\tilde{H}^{(n)}$, which differs from the eigenvector of the full Hamiltonian in the subset $S^{(n)}$. Note, that the initiator approximation used in the FCIQMC approach is a form of path filtering, and consequently, it introduces a source of error analogous to the path-filtering error.

III. IMPLEMENTATION

A. The PCI algorithm

The determinant selection procedure implemented via path filtering may be combined with the repeated application of the generator to obtain an approximate representation of the ground state wave function. In the case of the linear generator the resulting PCI algorithm consists of the following steps:

1. Trial wave function generation. The PCI procedure starts by selecting a trial wave function $\Omega^{(0)}$ to which corresponds the determinant space $S^{(0)}$. Although a convenient choice for the initial trial wave function $\Omega^{(0)}$ is the Hartree–Fock determinant Φ_{HF} , a CI with selected single and doubles out of Φ_{HF} yields faster convergence to the ground state.
2. Range estimation. The expectation value of the Hamiltonian with respect to the initial guess, $\langle \Omega^{(0)} | \hat{H} | \Omega^{(0)} \rangle$ is used to estimate an upper bound to the ground state energy E_0 . To estimate an upper bound to the energy of the highest excited state E_{N-1} , we employ Gershgorin’s circle theorem. Accordingly, we approximate the upper bound to the eigenvalues of \hat{H} as the sum of the diagonal element with the highest energy ($\langle \Phi_{N-1} | \hat{H} | \Phi_{N-1} \rangle$) plus the sum of the absolute values of the off-diagonal matrix elements that couple $|\Phi_{N-1}\rangle$ to other determinants:

$$\tilde{E}_{N-1} = \langle \Phi_{N-1} | \hat{H} | \Phi_{N-1} \rangle + \sum_I^{N-2} |\langle \Phi_{N-1} | \hat{H} | \Phi_I \rangle| \quad (34)$$

This estimate is not guaranteed to be a strict upper bound to E_{N-1} since it is possible that other Gershgorin circles might enclose energy ranges higher than the value of Eq. (34).

3. Propagation step. At step n , for each determinant $\Phi_J \in S^{(n)}$ loop over all the singly and doubly excited determinants Φ_I :

$$\Phi_I \in \{\hat{a}_a^\dagger \hat{a}_i \Phi_J, \hat{a}_a^\dagger \hat{a}_i^\dagger \hat{a}_j \hat{a}_i \Phi_J\} \quad (35)$$

where the indices i, j (a, b) label occupied (virtual) orbitals of Φ_J . For each determinant Φ_I , compute the thresholded spawning amplitude $[A_{IJ}^{(n+1)}(\eta)]$ according to Eq. (30) and add it to the wave function coefficient $\tilde{C}_I^{(n)}$:

$$\tilde{C}_I^{(n+1)} \leftarrow \tilde{C}_I^{(n+1)} + A_{IJ}^{(n+1)}(\eta) \quad (36)$$

Since the propagation step can be performed independently for each of the determinant in $S^{(n)}$, this section of the PCI algorithm may be easily parallelized by distributing the evaluation of $\tilde{C}_I^{(n+1)}$ over multiple threads/instances.

4. Normalization. The wave function at step $n + 1$ is normalized according to

$$C_I^{(n+1)} = \frac{\tilde{C}_I^{(n+1)}}{\|\tilde{C}^{(n+1)}\|_2} \quad \forall \Phi_I \in S^{(n+1)} \quad (37)$$

where $\|\tilde{C}^{(n+1)}\|_2$ is the 2-norm of the vector $\tilde{C}^{(n+1)}$.

5. Energy evaluation. The updated wave function coefficients are used to estimate the energy using two approaches. The first is the variational estimator $[E_{\text{var}}^{(n)}]$, which is given by the expectation value of the PCI wave function:

$$E_{\text{var}}^{(n)} = \langle \Omega^{(n)} | \hat{H} | \Omega^{(n)} \rangle = \sum_{IJ} C_I^{(n)} H_{IJ} C_J^{(n)} \quad (38)$$

The evaluation of E_{var} scales as $O^2 V^2 N_{\text{det}}$, where N_{det} is the number of determinants in $S^{(n)}$, therefore it has a computational cost comparable to that of applying \hat{H} without path filtering. Nevertheless, E_{var} is an upper bound to the exact ground state energy and the error is quadratic in the error of the wave function. To speed up the evaluation of E_{var} during the iterative procedure we apply numerical screening to the vector $C_I^{(n)}$.

We also compute the energy via the projective estimator $[E_{\text{proj}}^{(n)}]$, defined as:

$$E_{\text{proj}}^{(n)}(J) = H_{JJ} + \sum_{I(\neq J)} H_{IJ} \frac{C_I^{(n)}}{C_J^{(n)}} \quad (39)$$

where $H_{IJ} = \langle \Phi_J | \hat{H} | \Phi_I \rangle$ and Φ_J is chosen to be the determinant with the largest contribution to the wave function, that is, $J = \arg \max_I |C_I^{(n)}|$. E_{proj} may be evaluate with a cost proportional to $O^2 V^2$, where O and V are the number of occupied and virtual orbitals, respectively. However, the projective estimator is not variational and its error is linear in the wave function error. Consequently, the projective estimator is only used to monitor the convergence of the PCI algorithm.

6. Convergence check. Evaluate the approximate energy gradient:

$$\delta E^{(n+1)} = \frac{1}{\gamma} (E^{(n+1)} - E^{(n)}), \quad (40)$$

where γ is the convergence factor of the projector generator. If $|\delta E^{(n+1)}|$ is larger then the convergence threshold increase n by one and go to Step 2. Otherwise, the computation is converged and the final variational energy is evaluated including all contributions from the truncated CI space $S^{(n+1)}$.

The PCI algorithm is implemented in FORTE, a suite of multireference electronic structure methods⁸⁴ written as a plugin to the open-source quantum chemistry package Psi4.⁸⁵

IV. RESULTS

Unless otherwise noted, all the PCI calculations are performed with the 5th-order wall-Chebyshev generator.

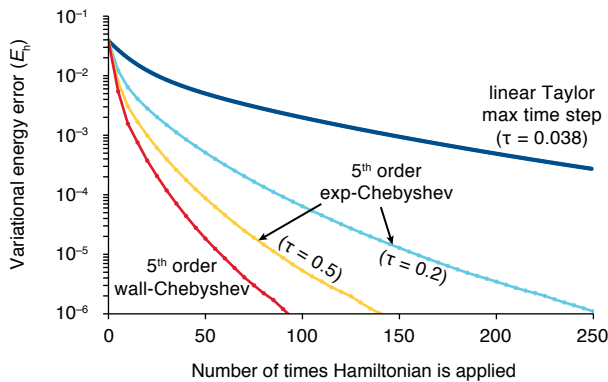


Figure 2. Ground state of N_2 at the equilibrium geometry ($r = 2.118$ bohr) computed with the PCI using a spawning threshold $\eta = 1 \times 10^{-5}$ and various projector generators. Difference between the variational energy at a given iteration and the converged energy as a function of the number of times the Hamiltonian is applied. All computations used canonical Hartree–Fock orbitals and the cc-pVDZ basis set. The 1s-like orbitals of nitrogen were excluded from computations of the correlation energy.

PCI results obtained with a spawning threshold equal to η are labeled as PCI(η). Preliminary computations showed that the variational estimator [Eq. (38)] yields energy errors that are consistently one order of magnitude smaller than those from the projective estimator [Eq. (39)]. Consequently, all results presented in this work are based on the variational energy estimator.

A. N_2

To investigate the properties of the PCI approach we report computations of the ground state energy of the nitrogen molecule using the cc-pVDZ basis set⁸⁶ and freezing the 1s core orbitals. We discuss both the equilibrium ($r = 2.118$ bohr) and stretched ($r = 4.2$ bohr) geometries of N_2 .

Figure 2 illustrates the difference in efficiency between various generator at the equilibrium geometry. To facilitate the comparison among the various generators, we plot the energy error with respect to the number of times \hat{H} is applied to a state vector using a spawning threshold equal to 10^{-5} . For the linear generator we select $\tau = 1/R = 0.038 E_h^{-1}$, the largest value of τ compatible with the spectral range of \hat{H} [see Eq. (17)]. As illustrated in Figure 2, the linear generator shows very slow convergence. After 250 steps, the total error is still larger than $10^{-4} E_h$. Projectors based on the exp-Chebyshev generators allow to use larger values of τ and converge more readily. For example, with $\tau = 0.5 E_h^{-1}$, the fifth-order exp-Chebyshev projector requires 150 applications of \hat{H} to achieve an error less than $10^{-6} E_h$. The fifth-order

wall-Chebyshev generator (which correspond to the limit $\tau \rightarrow \infty$) is more efficient than the exp-Chebyshev generators as it can achieve the same level of accuracy with less than 100 applications of \hat{H} .

Next, we study the accuracy of the PCI as a function of the spawning threshold (η) and compare it to a selection of single-reference and multireference methods. Table II reports a comparison of the total error with respect to FCI for the variational energy estimator [Eq. (38)]. Additionally, Table II reports energies for N_2 computed using second-order Møller–Plessett (MP2) perturbation theory, truncated CI with up to quadruple excitations (CISD–CISDTQ), coupled cluster with singles and doubles (CCSD), CCSD with perturbative triples corrections [CCSD(T)], uncontracted multireference CISD (MRCISD), and multireference CCSD (MR-CCSD) based on a CASSCF(6e,6o) reference.²⁵

From Table II it can be seen that since the PCI wave function is not biased towards a reference determinant, it can efficiently capture both static and dynamic electron correlation and provide an accurate description of N_2 at both equilibrium and stretched geometries. For example, even with a large spawning threshold ($\eta = 1 \times 10^{-3}$) the PCI yields a non-parallelism error (NPE, defined as the difference in energy error between the equilibrium and stretched geometries) that is of the order of a few mE_h . In contrast, single-reference approaches give NPEs that range from -322 to $+227 mE_h$.

The accuracy of the PCI is effectively tuned by the spawning threshold and can be chosen to match or go beyond that of MRCI and MRCC. For example, for $\eta = 2 \times 10^{-5}$, the NPE is equal to $0.37 \text{ kcal mol}^{-1}$, which is within chemical accuracy (defined as an error less than 1 kcal mol^{-1}). At the equilibrium geometry the PCI wave function has 1,264,528 determinants, with the Hartree–Fock determinant having a coefficient equal to 0.94. At the stretched geometry, when the coefficient of the Hartree–Fock determinant is only 0.46, this number increases to 2,628,056 determinants to accommodate the multideterminantal character of the wave function. Note that at both geometries the PCI(2×10^{-5}) wave function uses less than 0.5% of the FCI space determinants.

In order to illustrate the importance of the truncation and path-filtering errors, in Table II we report energies obtained by diagonalizing the Hamiltonian in the PCI determinant space (indicated as PCI+diag). These energies are more accurate than the corresponding PCI values. For example, with $\eta = 1 \times 10^{-4}$, the NPE for the PCI and PCI+diag are 5.7 and 1.2 mE_h , respectively. The difference between the energy from FCI and PCI+diag represents the truncation error, while the gap between the PCI and PCI+diag energies is the path-filtering error. For large spawning thresholds (e.g. $\eta = 1 \times 10^{-3}$) the truncation and path-filtering errors contribute equally to the total error. However, as the spawning threshold decreases, path-filtering becomes the dominant source of error. For example, when the spawning threshold is equal to 1×10^{-6} , the path-filtering error contributes to 90% of

Table II. Comparison of the ground state energy of N_2 computed with the PCI and several wave function approaches using the cc-pVDZ basis at equilibrium and stretched bond lengths ($r=2.118$ and 4.2 bohr). ΔE is the energy error with respect to FCI computed with the variational estimate. N_{par} is the number of variational parameters, with values in parentheses indicating the number of perturbative parameters. NPE is the non-parallelism error defined by the difference of energy errors between stretched and equilibrium geometries. All PCI computations use canonical restricted Hartree–Fock orbitals. The nitrogen $1s$ -like orbitals were frozen in all computations of the correlation energies.

Method	$r = 2.118$ bohr		$r = 4.2$ bohr		NPE/ mE_h
	N_{par}	$\Delta E/E_h$	N_{par}	$\Delta E/E_h$	
MP2	(2,090)	1.56×10^{-2}	(2,090)	-3.07×10^{-1}	-322.275
CISD	2,090	3.65×10^{-2}	2,090	2.64×10^{-1}	227.215
CISDT	60,842	2.59×10^{-2}	60,842	2.41×10^{-1}	215.173
CISDTQ	969,718	2.31×10^{-3}	969,718	5.72×10^{-2}	54.855
CCSD	2,090	1.45×10^{-2}	2,090	4.07×10^{-2}	26.234
CCSD(T)	(58,752)	1.87×10^{-3}	(58,752)	-1.65×10^{-1}	-166.876
MRCISD ^a	...	6.64×10^{-3}	...	6.91×10^{-3}	0.259
MRCCSD ^a	...	1.52×10^{-3}	...	2.25×10^{-3}	0.732
PCI(1×10^{-3})	12,393	2.45×10^{-2}	30,379	2.63×10^{-2}	1.816
PCI(1×10^{-4})	292,858	4.87×10^{-3}	573,665	1.06×10^{-2}	5.709
PCI(5×10^{-5})	532,728	3.08×10^{-3}	1,108,882	6.03×10^{-3}	2.952
PCI(2×10^{-5})	1,264,528	1.57×10^{-3}	2,628,056	2.25×10^{-3}	0.682
PCI(1×10^{-5})	2,703,218	8.76×10^{-4}	4,630,411	9.69×10^{-4}	0.093
PCI(1×10^{-6})	22,855,011	7.30×10^{-5}	32,900,610	8.82×10^{-5}	0.015
PCI(1×10^{-3})+diag ^b	12,393	1.32×10^{-2}	30,379	1.55×10^{-2}	2.276
PCI(1×10^{-4})+diag ^b	292,858	1.51×10^{-3}	573,665	2.68×10^{-3}	1.171
PCI(1×10^{-5})+diag ^b	2,703,218	1.68×10^{-4}	4,630,411	1.82×10^{-4}	0.014
PCI(1×10^{-6})+diag ^b	22,855,011	8.39×10^{-6}	32,900,610	9.12×10^{-6}	0.001
FCI	540,924,024		540,924,024		

^a MRCISD and MRCCSD data based on a CASSCF($6e,6o$) reference wave function were taken from Ref. 25.

^b The PCI+diag energies are computed by diagonalizing the Hamiltonian in the space of determinants obtained from a converged PCI computation.

the total error. In this case, the diagonalization of the PCI space yields energies within $10 \mu E_h$ from FCI values, while the nonparallelism error is about $1 \mu E_h$.

To give an idea of the computational cost of the PCI, we note that the N_2 computations at equilibrium geometry with $\eta = 10^{-6}$ ran in 3 hours on 16 threads on a single node (on two Intel Xeon E5-2650 v2 processors) and took 16 iterations to finish. The corresponding computation at the stretched geometry ran in 44 hours and took 127 iterations. In this example the wave function contains 33 million determinants and convergence is slowed by the small energy gap between the ground and first excited state.

B. C_2

To study the performance of PCI on larger basis sets we computed the ground state energy of C_2 at the equilibrium geometry using basis sets that range from double- to quadruple- ζ quality. Table III collects PCI results obtained using MP2 natural orbitals, together with trun-

cated configuration interaction, coupled cluster, DMRG, and i-FCIQMC results. When possible, computations were reported for the first three basis sets of the cc-pVXZ series ($X=D,T,Q$, also abbreviated as XZ in the following discussion).^{88,90} For the TZ and QZ basis sets the FCI energy cannot be computed, and we take DMRG results from Ref. 31 as a reference. PCI(η) energies are extrapolated to zero spawning threshold by fitting results with $\eta = 1 \times 10^{-5}$, 5×10^{-6} , and 1×10^{-6} to a quadratic function.

Table III illustrates how the PCI energy may be systematically converged to the reference FCI/DMRG energy with control over the absolute energy error. For example, with a spawning threshold equal to 10^{-5} , for all basis sets the PCI energy is within $1.3 mE_h$ from the DMRG energy. While with a spawning threshold equal to 10^{-6} , the error is further reduced to less than $0.2 mE_h$ in all cases.

When compared to other methods, the cheapest PCI calculations ($\eta = 10^{-4}$) shown in Tab. III are found to be already more accurate than truncated CI methods up to quadruple excitation and CCSD. Moreover, the PCI

Table III. Comparison of the ground state energy of C_2 calculated with the PCI and several wave function approaches using the cc-pVXZ basis set ($X = D, T, Q$). All PCI computations use MP2 natural orbitals. The carbon 1s-like orbitals were frozen in all calculations. N_{par} indicates the number of variational parameters, with values in parentheses indicating perturbative parameters. All results are shifted by $+75 E_h$.

Method	cc-pVDZ (8e, 26o)		cc-pVTZ (8e, 58o)		cc-pVQZ (8e, 108o)	
	$(E + 75)/E_h$	N_{par}	$(E + 75)/E_h$	N_{par}	$(E + 75)/E_h$	N_{par}
MP2	-0.697 678	(1.43×10^3)	-0.756 562	(8.35×10^3)	-0.777 234	(3.05×10^4)
CISD	-0.663 765	1.43×10^3	-0.711 300	8.35×10^3	-0.726 551	3.05×10^4
CISDT	-0.682 929	3.34×10^4	-0.733 939	4.96×10^5	-0.749 947	3.55×10^6
CISDTQ	-0.721 845	4.11×10^5	-0.777 182	1.51×10^7	-0.794 504	2.09×10^8
CCSD	-0.699 132	1.43×10^3	-0.749 551	8.35×10^3	-0.765 696	3.05×10^4
CCSD(T)	-0.726 697	(3.20×10^4)	-0.783 070	(4.88×10^5)	-0.800 807	(3.52×10^6)
PCI(1×10^{-4})	-0.725 914	1.58×10^5	-0.779 959	5.67×10^5	-0.796 216	1.00×10^6
PCI(5×10^{-5})	-0.727 131	3.09×10^5	-0.781 984	1.27×10^6	-0.798 720	2.40×10^6
PCI(1×10^{-5})	-0.728 292	1.22×10^6	-0.784 133	7.45×10^6	-0.801 450	1.67×10^7
PCI(5×10^{-6})	-0.728 439	2.03×10^6	-0.784 561	1.50×10^7	-0.801 973	3.65×10^7
PCI(1×10^{-6})	-0.728 541	5.56×10^6	-0.784 961	6.79×10^7	-0.802 513	1.99×10^8
PCI(extrapol.) ^a	-0.728 565		-0.785 069		-0.802 665	
DMRG ^{b,c}	-0.728 556	5.2×10^5	-0.785 054	1.2×10^7	-0.802 671	7.0×10^7
DMRG ^d	-0.802 69	...
i-FCIQMC ^{e,f}	-0.728 78	4.2×10^6	-0.784 93	6.3×10^6	-0.802 51	3.0×10^7
i-SFCIQMC ^{g,f}	-0.802 575	1.6×10^7
FCI ^h	-0.728 556	2.79×10^7	...	2.25×10^{10}	...	3.59×10^{12}

^a Extrapolated PCI values obtained from a quadratic fitting of the results with $\eta = 10^{-5}$, 5×10^{-6} , and 10^{-6} .

^b DMRG data taken from Ref. 31. Based on the genetic algorithm ordering and accurate to better than $0.01 mE_h$.

^c DMRG number of variational parameters were kindly provided by Guo and Chan⁸⁷ for computations with 946, 3234, and 6738 renormalized states using the DZ, TZ, and QZ basis sets, respectively.

^d DMRG data taken from Ref. 88. Based on the genetic algorithm ordering and accurate to better than $0.01 mE_h$.

^e Initiator FCIQMC (i-FCIQMC) data taken from Ref. 59.

^f For i-FCIQMC and i-SFCIQMC the column labeled N_{par} reports the total number of walkers.

^g Initiator semi-stochastic FCIQMC (i-SFCIQMC) data taken from Ref. 89.

^h The number of FCI determinants for the triple- and quadruple- ζ basis sets was estimated as $(\frac{N_{\text{orb}}}{N_{\text{el}}/2})^2 / N_{\text{irrep}}$, where N_{orb} , N_{el} , and N_{irrep} are the number of orbitals, electrons, and irreps, respectively.

selects the most important determinants efficiently and therefore shows a more favorable accuracy/(number of parameters) ratio. For example, the cc-pVQZ PCI($\eta = 10^{-4}$) wave function has about one million determinants, but yields an energy that is more accurate than that of CISDT (3 million determinants) and CISDTQ (200 million determinants). We note that PCI results surpass the accuracy of the CCSD(T) method with a spawning threshold of 1×10^{-5} .

The PCI shows a favorable scaling with respect to the size of basis set. When the basis set is enlarged from DZ to QZ, the number of orbitals involved in calculation grow from 26 to 108 and the corresponding FCI space increased ca. 10^5 folds. The corresponding growth of PCI determinants with respect to the number of virtual orbitals (n_{virt}) is found to be linear, with increase of only 14 and 36 times when $\eta = 1 \times 10^{-5}$ and 1×10^{-6} , respectively. In comparison, truncated CI and CC schemes scale as n_{virt}^2 , n_{virt}^3 , and n_{virt}^4 for the SD, SDT, and SDTQ truncation schemes, respectively. Consequently, the cost of these computations grows by a factor 21, 106, and 509 when going from the DZ to the QZ basis set. FCIQMC also

shows very good scaling with respect to virtual orbitals, with an increase of only about 7 times the number of walkers. In the case of DMRG, assuming that the number of renormalized states (M) required to obtain a given level of accuracy scales as $n_{\text{occ}} n_{\text{vir}}$,³¹ then the number of variational parameters scales as $n_{\text{orb}} M^2 \approx n_{\text{vir}}^3$.

We would like to point out that the QZ PCI calculation with spawning threshold 1×10^{-6} (200 million determinants) ran on a single node. This computation is two orders of magnitude larger than the largest selected CI calculations reported in the literature (4 million determinants),⁹¹ which was performed with a parallel algorithm on a distributed memory architecture with 32–256 nodes. As a comparison, typical FCIQMC computations may employ up to 2–7 billion walkers.⁵⁷

C. Size consistency and molecular orbital comparison

Lastly, we investigate the degree to which the PCI wave function lacks size consistency, and how different type of molecular orbitals affect its performance. In our

Table IV. Analysis of the size consistency error (ΔE) of truncated CI methods and the PCI for the $(\text{Be-He})_2$ system. All results used the cc-pVDZ and STO-3G basis sets for Be and He, respectively. The Be-He bond distance in the monomer is equal to 2.5 Å. The column labeled N_{det} reports the size of each CI space.

Method	Be-He (6e,15o)		He-Be \cdots Be-He (12e,30o)		$\Delta E/mE_h$
	Energy/ E_h	N_{det}	Energy/ E_h	N_{det}	
RHF	-17.374 136	1	-34.748 272	1	0.000
FCI	-17.420 556	51,853	-34.841 113	4.41×10^{10}	0.000
CISD	-17.420 420	523	-34.833 525	4,405	7.316
CISDT	-17.420 484	4,257	-34.833 664	170,685	7.305
CISDTQ	-17.420 556	17,973	-34.841 084	3,833,121	0.029
Delocalized canonical Hartree-Fock orbitals					
PCI(1×10^{-4})	-17.420 537	1,424	-34.840 544	34,164	0.529
PCI(1×10^{-5})	-17.420 556	5,311	-34.841 066	255,342	0.045
PCI(1×10^{-6})	-17.420 556	15,465	-34.841 108	1,558,745	0.005
Delocalized MP2 natural orbitals					
PCI(1×10^{-4})	-17.420 547	1,138	-34.840 924	23,979	0.169
PCI(1×10^{-5})	-17.420 556	5,077	-34.841 088	163,469	0.024
PCI(1×10^{-6})	-17.420 556	14,801	-34.841 110	1,185,988	0.002
Localized canonical Hartree-Fock orbitals					
PCI(1×10^{-4})	-17.420 537	1,424	-34.840 981	9,746	0.092
PCI(1×10^{-5})	-17.420 556	5,311	-34.841 104	60,740	0.007
PCI(1×10^{-6})	-17.420 556	15,465	-34.841 112	337,662	0.001
Localized MP2 natural orbitals					
PCI(1×10^{-4})	-17.420 547	1,138	-34.841 064	5,910	0.029
PCI(1×10^{-5})	-17.420 556	5,077	-34.841 109	41,580	0.003
PCI(1×10^{-6})	-17.420 556	14,801	-34.841 113	247,364	0.000

tests we have considered a monomer consisting of Be and He separated by 2.5 Å. In one set of computations two monomers are arranged in a $D_{\infty h}$ geometry, so that the orbitals are delocalized over the two fragments. Starting from the $D_{\infty h}$ geometry, we obtained a $C_{\infty v}$ structure in which the Be-He distances of the monomers are shortened and lengthened by $\pm 10^{-5}$ Å, respectively. This geometric change leads to localization of the molecular orbitals on one of the two monomers. For both localized and delocalized molecular orbitals we considered canonical Hartree-Fock orbitals and MP2 natural orbitals.

Table IV reports the size consistency error (ΔE) for a pair of noninteracting Be-He units as a function of the spawning threshold, where ΔE is defined as the energy difference between a non-interacting dimer (Be-He \cdots Be-He) and twice the energy of the monomer (Be-He):

$$\Delta E = E(\text{Be-He} \cdots \text{Be-He}) - 2E(\text{Be-He}). \quad (41)$$

As expected, the PCI energy is not size consistent, but a comparison with truncated CI methods shows that the corresponding error is significantly smaller in the case of PCI and can be effectively controlled via the spawning threshold. In comparison to CISDTQ, which requires 3,833,121 determinants for the dimer computation, the PCI(10^{-6}) with canonical orbitals requires only 1,558,745

determinants and leads to a size consistency error that is six times smaller. When delocalized orbitals are used, going from canonical Hartree-Fock orbitals to MP2 natural orbitals leads to a reduction of the size consistency error of the PCI by a factor of ca. two. At the same time, the use of MP2 natural orbitals also slightly reduces the number of determinants.

Upon localization of the orbitals we observe a significant reduction of the size consistency error and wave function size. For example, localization of the canonical Hartree-Fock orbitals reduces the PCI(10^{-6}) size consistency error and number of determinants by a factor of five. The best performance is obtained by combining localization with MP2 natural orbitals. In this case the overall size of the PCI wave function is reduced by a factor of 6 and the size consistency error is less than 0.001 mE_h . This comparison shows that the use of optimized orbitals can significantly reduce the computational cost of the PCI and the magnitude of the size consistency error.

V. SUMMARY AND CONCLUSIONS

In this paper, we introduced a general projector diagonalization approach and combined it with path filter-

ing to create a novel projector configuration interaction (PCI) method. Given an operator (matrix) \hat{H} , the projector diagonalization method seeks to obtain one of the eigenvectors of \hat{H} via repeated application of the projector generator $g(\hat{H})$ onto a trial vector. The projector generator is a matrix function designed to amplify the coefficient of one of the eigenvectors. The focus of this work is on polynomial projector generators derived from the imaginary-time propagator, which project the trial wave function onto the ground electronic state. To improve the performance of a Taylor expansion of the imaginary-time propagator, we discuss its approximation in terms of Chebyshev polynomials, and propose a new generator (wall-Chebyshev) with superior convergence properties.

The PCI optimization process is formulated in terms of a dynamics in which each application of the projector generator is equivalent to a spawning process. In this process, each determinant spawns singly and doubly excited determinants with a given spawning amplitude. In order to truncate the determinant space explored by the PCI algorithm, we consider a path filtering approach in which spawning amplitudes are truncated according to a user-provided *spawning threshold* (η). Path filtering applied at each step of the projector diagonalization controls the size of the PCI wave function and the accuracy of the energy by selecting important determinants that contribute the most to a given eigenstate. In this respect, the PCI method is similar to selected CI, with the important difference that the former also approximates the diagonalization process to increase computational efficiency.

Since the PCI is not biased towards any reference determinants, it can describe dynamic and static electron correlation equally well. This point is illustrated with computations of the energy of N_2 at equilibrium and stretched geometries. As shown in Table II, the PCI ($\eta = 2 \times 10^{-5}$) can predict the energy difference between these two geometries with a non-parallelism error equal to 0.682 mE_h ($0.43 \text{ kcal mol}^{-1}$) using only a small fraction of the Hilbert space of determinants (less than 0.5%). Additionally, we compare PCI with DMRG and FCIQMC using the carbon dimer as a challenging benchmark. With a spawning threshold equal to 10^{-6} , the PCI can match the accuracy of FCIQMC results, while PCI extrapolated to the limit $\eta \rightarrow 0$ yields total energies that are within 0.01 mE_h of DMRG reference data. We have also analyzed the extent of size consistency errors in PCI computations. This error is effectively controlled by the spawning threshold and may be further reduced by using a localized basis.

One of the interesting features of the PCI algorithm is that it can be expressed as a series of update steps in which spawning amplitudes for different determinants can be computed independently with no communication. Moreover, the linear and wall-Chebyshev generators only require storage of two vectors of the size of the CI space. These two features make the PCI amenable to computations with large CI spaces containing 10^7 –

10^8 determinants. A parallel implementation of the PCI for distributed-memory machines would allow to further increase the size of the CI space. Both the PCI and FCIQMC use a sparse representation of the FCI wave function and present similar challenges when implemented on distributed memory architectures. Therefore, the recent successful implementation of a parallel FCIQMC code⁶³ suggests that it should be possible to also produce an efficient parallel implementation of the PCI.

Currently, the PCI algorithm has been formulated to optimize the ground state. However, several strategies may be explored to extend the PCI to electronic excited states. One possibility is a state-specific approach in which excited states are optimized individually, while maintaining orthogonality with lower energy states. An alternative is a multistate version of the PCI in which several states are optimized simultaneously.⁹² Since the convergence of the PCI depends on ratio of the first excitation energy and the spectral radius, $(E_1 - E_0)/R$, a multistate version of the PCI would also be helpful to speed up convergence to the ground state in cases when this ratio is small. Another interesting venue to explore is to use the PCI approach to target the density matrix at finite temperatures^{93,94} or to compute approximate spectral densities of systems with a dense manifold of low-energy electronic states.⁹⁵

Appendix A: Path filtering for polynomial generators

In this appendix we report a generalization of the path filtering approach for polynomial generators $g(x)$ of order m that have m real roots ($s_i, i = 1, \dots, m$). In this case, $g(x)$ can be written as:

$$g(x) = \prod_{i=1}^m \frac{x - s_i}{E_0 - s_i} \quad (\text{A1})$$

and $g(\hat{H})|\Omega^{(n)}\rangle$ may be computed by repeated application of a linear generator with modified shift to which path filtering is applied in all intermediate steps. It is important to point out that the path-filtering algorithm presented here gives results that are consistent with those of the algorithm outlined in the paper, which applies only to linear generators.

For convenience, we start by defining a series of normalized trial wave functions

$$|\Omega^{(n+1,i)}\rangle = \sum_{I \in S^{(n,i)}} C_I^{(n+1,i)} |\Phi_I\rangle \quad (\text{A2})$$

expanded over the space $S^{(n,i)}$. The coefficient vector for $i = 0$ is given by:

$$C_I^{(n+1,0)} = C_I^{(n)} \quad (\text{A3})$$

and spans the space $S^{(n+1,0)} = S^{(n)}$.

The coefficients $C_I^{(n+1,i)}$ for $i > 0$ are obtained from the unnormalized wave function coefficients $[\tilde{C}_I^{(n+1,i)}]$:

$$C_I^{(n+1,i)} = \frac{\tilde{C}_I^{(n+1,i)}}{\|\tilde{C}^{(n+1,i)}\|_2} \quad (\text{A4})$$

which are obtained as the sum:

$$\tilde{C}_I^{(n+1,i)} = \sum_{\Phi_J \in S^{(n+1,i)}} A_{IJ}^{(n+1,i)}(\eta) \quad (\text{A5})$$

The path-filtered spawning amplitudes $[A_{IJ}^{(n,i)}(\eta)]$ that enter into Eq. (A5) are obtained from the untruncated amplitudes $[A_{IJ}^{(n,i)}]$:

$$A_{IJ}^{(n,i)} = \langle \Phi_I | \hat{H} - s_i | \Phi_J \rangle C_J^{(n,i-1)} \quad (\text{A6})$$

and truncated according to:

$$A_{IJ}^{(n,i)}(\eta) = \begin{cases} A_{II}^{(n,i)} & \text{if } I = J \\ A_{IJ}^{(n,i)} \Theta(|A_{IJ}^{(n,i)}| - \eta) & \text{if } I \neq J \end{cases} \quad (\text{A7})$$

The normalized coefficients are evaluated recursively for $i = 1, 2, \dots, m$ following Eqs. (A4)–(A7). Finally, the coefficients for the updated wave function are given by:

$$C_I^{(n+1)} = C_I^{(n+1,m)}. \quad (\text{A8})$$

Note that to evaluate the application of factorizable generators with real zeros onto a trial vector requires storage of two vectors. Thus, require the same amount of memory as the linear projector.

ACKNOWLEDGMENTS

The authors are grateful to Philip Shushkov and Michele Benzi for valuable discussions concerning the theory of projectors. The authors would also like to thank Sheng Guo and Garnet Chan for providing the number of wave function parameters for the DMRG computations on the carbon dimer.

This work was supported by start-up funds provided by Emory University.

REFERENCES

- ¹C. D. Sherrill and H. F. Schaefer III, *Adv. Quant. Chem.* **34**, 143 (1999).
- ²E. Rossi, G. L. Bendazzoli, S. Evangelisti, and D. Maynau, *Chem. Phys. Lett.* **310**, 530 (1999).
- ³P. J. Knowles and N. C. Handy, *J. Chem. Phys.* **91**, 2396 (1989).
- ⁴R. J. Bartlett and M. Musial, *Rev. Mod. Phys.* **79**, 291 (2007).
- ⁵R. J. Bartlett, *Annu. Rev. Phys. Chem.* **32**, 359 (1981).
- ⁶E. Dagotto, *Science* **309**, 257 (2005).
- ⁷R. J. Buenker and S. D. Peyerimhoff, *Theor. Chim. Acta* **35**, 33 (1974).
- ⁸R. J. Buenker and S. D. Peyerimhoff, *Theor. Chim. Acta* **39**, 217 (1975).
- ⁹B. Huron, J. P. Malrieu, and P. Rancurel, *J. Chem. Phys.* **58**, 5745 (1973).
- ¹⁰S. Evangelisti, J.-P. Daudey, and J.-P. Malrieu, *Chem. Phys.* **75**, 91 (1983).
- ¹¹J. Meller, J. Heully, and J. Malrieu, *Chem. Phys. Lett.* **218**, 276 (1994).
- ¹²C. F. Bender and E. R. Davidson, *Phys. Rev.* **183**, 23 (1969).
- ¹³S. R. Langhoff, S. T. Elbert, and E. R. Davidson, *Int. J. Quant. Chem.* **7**, 999 (1973).
- ¹⁴C. Angeli, R. Cimiraglia, M. Persico, and A. Toniolo, *Theor. Chem. Acc.* **98**, 57 (1997).
- ¹⁵C. Angeli and M. Persico, *Theor. Chem. Acc.* **98**, 117 (1997).
- ¹⁶C. Angeli, R. Cimiraglia, and M. Persico, *Theor. Chem. Acc.* **100**, 324 (1998).
- ¹⁷J. Olsen, B. O. Roos, P. Jørgensen, and H. J. A. Jensen, *J. Chem. Phys.* **89**, 2185 (1988).
- ¹⁸J. Ivanic, *J. Chem. Phys.* **119**, 9364 (2003).
- ¹⁹D. Ma, G. Li Manni, and L. Gagliardi, *J. Chem. Phys.* **135**, 044128 (2011).
- ²⁰G. Li Manni, D. Ma, F. Aquilante, J. Olsen, and L. Gagliardi, *J. Chem. Theory Comput.* **9**, 3375 (2013).
- ²¹J. B. Schriber and F. A. Evangelista, *J. Chem. Phys.* **144**, 161106 (2016).
- ²²S. R. White, *Phys. Rev. Lett.* **69**, 2863 (1992).
- ²³S. R. White and R. L. Martin, *J. Chem. Phys.* **110**, 4127 (1999).
- ²⁴G. K.-L. Chan and M. Head-Gordon, *J. Chem. Phys.* **116**, 4462 (2002).
- ²⁵G. K.-L. Chan, M. Kállay, and J. Gauss, *J. Chem. Phys.* **121**, 6110 (2004).
- ²⁶Y. Kurashige and T. Yanai, *J. Chem. Phys.* **130**, 234114 (2009).
- ²⁷W. Mizukami, Y. Kurashige, and T. Yanai, *J. Chem. Theory Comput.* **9**, 401 (2012).
- ²⁸Y. Kurashige and T. Yanai, *Bull. Chem. Soc. Japan* **87**, 1071 (2014).
- ²⁹Y. Kurashige, G. K.-L. Chan, and T. Yanai, *Nature Chem.* **5**, 660 (2013).
- ³⁰G. H. Booth and G. K.-L. Chan, *J. Chem. Phys.* **137**, 191102 (2012).
- ³¹R. Olivares-Amaya, W. Hu, N. Nakatani, S. Sharma, J. Yang, and G. K. Chan, *J. Chem. Phys.* **142**, 034102 (2015).
- ³²G. Vidal, *Phys. Rev. Lett.* **99**, 220405 (2007).
- ³³N. Nakatani and G. K.-L. Chan, *J. Chem. Phys.* **138**, 134113 (2013).
- ³⁴H. Nakano and K. Hirao, *Chem. Phys. Lett.* **317**, 90 (2000).
- ³⁵S. M. Parker, T. Seideman, M. A. Ratner, and T. Shiozaki, *J. Chem. Phys.* **139**, 021108 (2013).
- ³⁶S. M. Parker and T. Shiozaki, *J. Chem. Phys.* **141**, 211102 (2014).
- ³⁷V. Murg, F. Verstraete, R. Schneider, P. R. Nagy, and Ö. Legeza, *J. Chem. Theory Comput.* (2015).
- ³⁸S. Szalay, M. Pfeffer, V. Murg, G. Barcza, F. Verstraete, R. Schneider, and Ö. Legeza, *Int. J. Quantum Chem.* **115**, 1342 (2015).
- ³⁹K.-H. Böhm, A. A. Auer, and M. Espig, *J. Chem. Phys.* **144**, 244102 (2016).
- ⁴⁰N. J. Mayhall, P. R. Horn, E. J. Sundstrom, and M. Head-Gordon, *Phys. Chem. Chem. Phys.* **16**, 22694 (2014).

- ⁴¹D. W. Small, K. V. Lawler, and M. Head-Gordon, *J. Chem. Theory Comput.* **10**, 2027 (2014).
- ⁴²T. Stein, T. M. Henderson, and G. E. Scuseria, *J. Chem. Phys.* **140**, 214113 (2014).
- ⁴³I. W. Bulik, T. M. Henderson, and G. E. Scuseria, *J. Chem. Theory Comput.* **11**, 3171 (2015).
- ⁴⁴T. Tsuchimochi and G. E. Scuseria, *J. Chem. Phys.* **131**, 121102 (2009).
- ⁴⁵C. A. Jiménez-Hoyos, T. M. Henderson, T. Tsuchimochi, and G. E. Scuseria, *J. Chem. Phys.* **136**, 164109 (2012).
- ⁴⁶R. Rodríguez-Guzmán, C. A. Jiménez-Hoyos, R. Schutski, and G. E. Scuseria, *Phys. Rev. B* **87**, 235129 (2013).
- ⁴⁷J. C. Greer, *J. Chem. Phys.* **103**, 1821 (1995).
- ⁴⁸J. Coe, P. Murphy, and M. Paterson, *Chem. Phys. Lett.* **604**, 46 (2014).
- ⁴⁹J. P. Coe and M. J. Paterson, *J. Chem. Phys.* **139**, 154103 (2013).
- ⁵⁰J. Coe and M. Paterson, *J. Chem. Phys.* **137**, 204108 (2012).
- ⁵¹W. Gyorffy, R. J. Bartlett, and J. C. Greer, *J. Chem. Phys.* **129**, 064103 (2008).
- ⁵²G. Sugiyama and S. Koonin, *Ann. Phys.* **168**, 1 (1986).
- ⁵³M. Honma, T. Mizusaki, and T. Otsuka, *Phys. Rev. Lett.* **75**, 1284 (1995).
- ⁵⁴W. Al-Saidi, S. Zhang, and H. Krakauer, *J. Chem. Phys.* **124**, 224101 (2006).
- ⁵⁵Y. Ohtsuka and S. Nagase, *Chem. Phys. Lett.* **463**, 431 (2008).
- ⁵⁶H. Shi and S. Zhang, *Phys. Rev. B* **88**, 125132 (2013).
- ⁵⁷G. H. Booth, A. J. W. Thom, and A. Alavi, *J. Chem. Phys.* **131**, 054106 (2009).
- ⁵⁸D. Cleland, G. H. Booth, and A. Alavi, *J. Chem. Phys.* **132**, 041103 (2010).
- ⁵⁹G. H. Booth, D. Cleland, A. J. W. Thom, and A. Alavi, *J. Chem. Phys.* **135**, 084104 (2011).
- ⁶⁰D. M. Cleland, G. H. Booth, and A. Alavi, *J. Chem. Phys.* **134**, 024112 (2011).
- ⁶¹D. Cleland, G. H. Booth, C. Overy, and A. Alavi, *J. Chem. Theory Comput.* **8**, 4138 (2012).
- ⁶²R. E. Thomas, C. Overy, G. H. Booth, and A. Alavi, *J. Chem. Theory Comput.* **10**, 1915 (2014).
- ⁶³G. H. Booth, S. D. Smart, and A. Alavi, *Mol. Phys.* **112**, 1855 (2014).
- ⁶⁴M. Imada and T. Kashima, *J. Phys. Soc. Jpn.* **69**, 2723 (2000).
- ⁶⁵Y. Imai, Y. Otsuka, and M. Imada, *J. Phys. Condens. Matter* **19**, 365230 (2007).
- ⁶⁶J. R. McClean and A. Aspuru-Guzik, *RSC Adv.* **5**, 102277 (2015).
- ⁶⁷F. Petruzielo, A. Holmes, H. J. Changlani, M. Nightingale, and C. Umrigar, *Phys. Rev. Lett.* **109**, 230201 (2012).
- ⁶⁸N. S. Blunt, S. D. Smart, J. A. Kersten, J. S. Spencer, G. H. Booth, and A. Alavi, *J. Chem. Phys.* **142**, 184107 (2015).
- ⁶⁹C. Umrigar, *J. Chem. Phys.* **143**, 164105 (2015).
- ⁷⁰N. M. Tubman, J. Lee, T. Y. Takeshita, M. Head-Gordon, and K. B. Whaley, arXiv:1603.02686 (2016).
- ⁷¹R. Kosloff and H. Tal-Ezer, *Chem. Phys. Lett.* **127**, 223 (1986).
- ⁷²W. Zhu, Y. Huang, D. Kouri, C. Chandler, and D. K. Hoffman, *Chem. Phys. Lett.* **217**, 73 (1994).
- ⁷³D. J. Kouri, W. Zhu, G. A. Parker, and D. K. Hoffman, *Chem. Phys. Lett.* **238**, 395 (1995).
- ⁷⁴G. A. Parker, W. Zhu, Y. Huang, D. K. Hoffman, and D. J. Kouri, *Comput. Phys. Commun.* **96**, 27 (1996).
- ⁷⁵R. Chen and H. Guo, *Comput. Phys. Commun.* **119**, 19 (1999).
- ⁷⁶J. P. Boyd, *Chebyshev and Fourier spectral methods* (Dover Publications, Inc., Mineola, New York, USA, 2001).
- ⁷⁷D. Horn and M. Weinstein, *Phys. Rev. D* **30**, 1256 (1984).
- ⁷⁸E. Sim and N. Makri, *Comput. Phys. Commun.* **99**, 335 (1997).
- ⁷⁹E. Sim and N. Makri, *J. Phys. Chem. B* **101**, 5446 (1997).
- ⁸⁰N. Makri, *Annu. Rev. Phys. Chem.* **50**, 167 (1999).
- ⁸¹R. Lambert and N. Makri, *J. Chem. Phys.* **137**, 22A553 (2012).
- ⁸²D. E. Amos, *Math. Comp.* **28**, 239 (1974).
- ⁸³A. A. Holmes, H. J. Changlani, and C. J. Umrigar, *J. Chem. Theory Comput.* **12**, 1561 (2016).
- ⁸⁴Forté, a suite of quantum chemistry methods for strongly correlated electrons. For current version see <https://github.com/evangelistalab/forte> (2016).
- ⁸⁵J. M. Turney, A. C. Simmonett, R. M. Parrish, E. G. Hohenstein, F. A. Evangelista, J. T. Fermann, B. J. Mintz, L. A. Burns, J. J. Wilke, M. L. Abrams, N. J. Russ, M. L. Leininger, C. L. Janssen, E. T. Seidl, W. D. Allen, H. F. Schaefer, R. A. King, E. F. Valeev, C. D. Sherrill, and C. T. Daniel, *WIREs: Comput. Mol. Sci.* **2**, 556 (2012).
- ⁸⁶T. H. Dunning, *J. Chem. Phys.* **90**, 1007 (1989).
- ⁸⁷S. Guo and G. K.-L. Chan, (personal communication, 2016).
- ⁸⁸S. Sharma, *J. Chem. Phys.* **142**, 024107 (2015).
- ⁸⁹N. S. Blunt, S. D. Smart, G. H. Booth, and A. Alavi, *J. Chem. Phys.* **143**, 134117 (2015).
- ⁹⁰R. A. Kendall, T. H. Dunning Jr, and R. J. Harrison, *J. Chem. Phys.* **96**, 6796 (1992).
- ⁹¹P. Stampfuss and W. Wenzel, *J. Chem. Phys.* **122**, 024110 (2005).
- ⁹²S. Ten-no, *J. Chem. Phys.* **138**, 164126 (2013).
- ⁹³N. S. Blunt, T. W. Rogers, J. S. Spencer, and W. M. C. Foulkes, *Phys. Rev. B* **89**, 245124 (2014).
- ⁹⁴F. D. Malone, N. S. Blunt, J. J. Shepherd, D. K. K. Lee, J. S. Spencer, and W. M. C. Foulkes, *J. Chem. Phys.* **143**, 044116 (2015).
- ⁹⁵L. Lin, Y. Saad, and C. Yang, *SIAM Rev.* **58**, 34 (2016).